minerals

MDPI

Article

HAp/β-TCP Biphasic Ceramics Obtained by the Pechini Method: An Antibacterial Approach

Geysivana K. Carvalho [1], José R. S. Farias [2], Idglan S. Lima [1], Ariane M. Nascimento [1], Gelmires A. Neves [3], Romualdo Menezes [3], Josy A. Osajima [1], Aluska Braga [2,4,*] and Edson C. Silva-Filho [1,*]

[1] Interdisciplinary Laboratory of Advanced Materials, Federal University of Piauí, Teresina 64064-260, Brazil
[2] Development Laboratory of Ceramic materials (LaDeC), Federal University of Piauí, Teresina 64049-550, Brazil
[3] Academic Unit of Materials Engineering, Federal University of Campina Grande, Campina Grande 58429-900, Brazil
[4] Postgraduate in Materials Engineering at the Federal Institute of Education, Science, and Technology of Piauí (PPGEM-IFPI), Teresina 64000-040, Brazil
* Correspondence: aluskasimoes@ufpi.edu.br (A.B.); edsonfilho@ufpi.edu.br (E.C.S.-F.)

Abstract: Calcium phosphates (CaPs) have broad applications in biomedicine, with the most used phases being hydroxyapatite (HAp) and β-tricalcium phosphate (β-TCP) due to their similarity with natural bone. There are several methods for obtaining CaPs. However, the Pechini method attracts much attention due to its advantages: homogeneous molecular mixing, obtaining nanocrystalline particles, low processing temperature, generating nanometric particles, and simplicity. However, this method is little discussed for the synthesis of CaPs. This work aimed to synthesize CaPs using the Pechini method, analyzing the antibacterial properties. The samples were characterized by X-ray diffraction (XRD), Fourier-transform infrared spectroscopy (FTIR), thermogravimetric analysis (TG/DTG), scanning electron microscopy (SEM), and energy dispersive spectroscopy (EDS). The XRD confirmed obtaining the biphasic ceramic of HAp, with no other phase as an impurity, where the ratio between citric acid and ethylene glycol (AC/EG) influenced the percentage of HAp phases and β-TCP formed. Thermogravimetric analysis showed a mass loss of approximately 7%. SEM observed the formation of post-agglomerates and irregular shapes. The bacteriological test was satisfactory. The samples showed above 25% inhibition for the growth of *Staphylococcus aureus* and *Escherichia coli* bacteria.

Keywords: calcium phosphate; antimicrobial; characterization

Citation: Carvalho, G.K.; Farias, J.R.S.; Lima, I.S.; Nascimento, A.M.; Neves, G.A.; Menezes, R.; Osajima, J.A.; Braga, A.; Silva-Filho, E.C. HAp/β-TCP Biphasic Ceramics Obtained by the Pechini Method: An Antibacterial Approach. *Minerals* **2022**, *12*, 1482. https://doi.org/10.3390/min12121482

Academic Editor: Huaming Yang

Received: 13 September 2022
Accepted: 15 November 2022
Published: 22 November 2022

1. Introduction

The use of biomaterials for the recovery or replacement of bone tissue has become a routine procedure in medicine and dentistry, necessary in applications such as the coating or construction of prostheses, healing fractures, or filling significant bone defects [1,2]. In the last few decades, researchers have studied different biomaterials related to developing a new material that constitutes the ideal bone graft substitute [3]. As a result, several biological materials, such as calcium phosphate (CaP) bioceramics, have been developed and used, due to their excellent biocompatibility with bone tissue and their chemical similarity with the mineral content of bones [4].

Hydroxyapatite (HAp) ($Ca_{10}(PO_4)_6(OH)_2$) is a well-known calcium phosphate belonging to the apatite family, being widely explored in the biomedical area due to its characteristics: structure similar to bone mineral, biocompatibility, osteoconduction, stability concerning bioabsorption and being non-toxic [5], having a molar ratio Ca/P 1.67 [6]. However, pure HAp has the disadvantage of slow biodegradation during the repair of bone defects. Therefore, to avoid failure or slow reaction of materials with bone tissues,

selecting appropriate phases is essential to maintain the balance of material dissolution and new bone formation [7].

β-Tricalcium phosphate (β-TCP) has also received much attention for use as a substitute for bone graft, as it gradually dissolves to leave some pores for the bone formation of the new biological host and accelerates the process of apatite precipitation [8]. In addition, the mixture of HAp and β-TCP produces biphasic calcium phosphate (BCP), which has the reactivity of β-TCP and the stability of HAp, providing more bioactivity, increasing bone growth, and ensuring better resistance of implants to tension [9].

Recently, several synthesis routes for producing CaP powders have been developed [10]. In this way, the application of the material must be well known to use the best synthesis route to achieve the desired properties. The chemical precipitation, solid-state reaction, and sol-gel methods are examples of traditional synthesis routes widely used to obtain CaP powders. However, such methods have several disadvantages, such as a low degree of chemical homogeneity, more significant contamination, long processing time, formation of cracks during heat treatment, and permanence of fine residual pores, among others [11]. The Pechini method is an alternative for synthesizing calcium phosphate powders, which has gained prominence compared to conventional methods. Because it allows the use of different temperature ranges, different proportions of citric acid and metallic cations allows changing the variables used in the process and controlling the stoichiometry of the samples. It also allows better kinetics of crystallization and growth of the particles through ethylene glycol used as a solvent for the polymerization process between citric acid and metallic cations [12].

Despite such attractions, this method has yet to be studied for synthesizing calcium phosphate powders. Peña and Vallet-Regi [13] synthesized several phases of calcium phosphates via the Pechini method, including hydroxyapatite and α- and β-tricalcium phosphates. Nine compositions, varying the Ca/P molar ratio between 1.5 and 1.667, were synthesized. Solutions were prepared in an aqueous medium using a citric acid and ethylene glycol ratio of 1:1. When the Ca/P ratio was 1.667, and with heat treatment at 1000 °C/24 h, monophasic hydroxyapatite was obtained.

Omori et al. [6] studied the synthesis of the hydroxyapatite phase by the Pechini method, also under non-stoichiometric conditions. The authors studied two synthesis routes: the first used calcium nitrate, monobasic ammonium phosphate, citric acid, and ethylene glycol as reagents. Two molar ratios of Ca/P were studied, and the formation of phases of HAp, CaO, and β-TCP was observed in the ratio Ca/P = 1.67. They used the same reagents in the second route but replaced calcium nitrate with calcium acetate and ethylene glycol with poly (acrylic acid). In this second route, different Ca/P molar conditions were studied. All samples obtained exhibited the formation of two phases, HAp and CaO.

Thus, although calcium phosphates are extensively studied in the literature, there is a scarcity of research that uses the Pechini method to obtain them and studies that enable the use of CaPs produced by this route. This work aims to synthesize CaP powders by the Pechini method, studying the influence of the ratio between citric acid and ethylene glycol (AC/EG) in the synthesis and evaluating the antibacterial activity of the materials against two strains.

2. Materials and Methods

2.1. Materials

High-purity reagents were used, including anhydrous citric acid—$C_6H_8O_7$ (Cinética, Itapevi, São Paulo, Brazil), calcium nitrate—$Ca(NO_3)_2{\cdot}4H_2O$ (Itapevi, São Paulo, Brazil), diammonium hydrogen phosphate—$(NH_4)_2HPO_4$ (Neon, Suzano, São Paulo, Brazil), ethylene glycol—$HOCH_2CH_2OH$ (LabSynth, Diadema, São Paulo, Brazil), and deionized water (Federal University of Piauí, Teresina Piauí, Brazil). All analytical reagents were used without purification.

2.2. Synthesis of Bioceramics by the Pechini Method

Firstly, 100 mL of deionized water was added under constant stirring at 70 °C. Next, the citric acid (30.63 g), calcium nitrate (11.76 g), and ammonium phosphate dibasic (3.95 g) were added separately to the solution until completely dissolved. A 2:1 ratio between citric acid and metal cations (AC/CM) was used. In the esterification and polyesterification reactions, ethylene glycol (EG) was added (indicate the amount), then the temperature was raised to 120 °C, forming the gel. The proportions of citric acid and ethylene glycol (AC/EG) varied at 40:60, 50:50, and 60:40.

The resin formed underwent heat treatment (pyrolysis) in a muffle furnace at a temperature of 400 °C/1 h with a heating rate of 10 °C/min. The puff formed was de-agglomerated and sieved through an ABNT No. 200 sieve with a mesh diameter of 0.074 mm. The resulting powder was calcined at 1000 °C, with a heating rate of 10 °C/min for 1 h, to form the bioceramic. The nomenclature adopted to describe the synthesized samples was as follows: BCP, which means biphasic calcium phosphate, followed by the variation between citric acid and ethylene glycol of 40, 50, or 60, when this ratio was 40/60, 50/50, and 60/40, respectively. The synthesis scheme is shown in Figure 1.

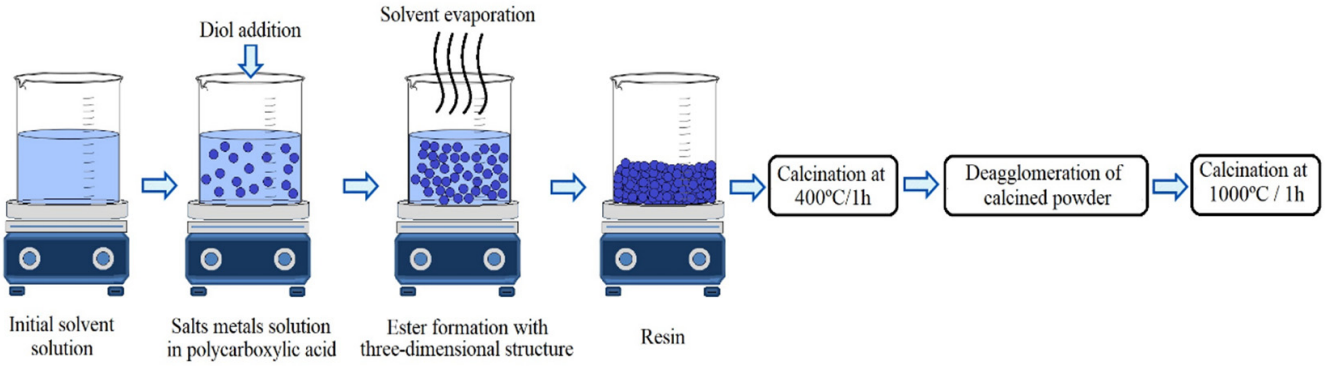

Figure 1. Synthesis representation.

2.3. Characterization

The synthesized samples were characterized by X-ray diffraction to identify the phases formed, quantify the phases, and calculate the percentage of crystallinity and crystallite size. The diffractograms of the samples were created in Shimadzu equipment, model XRD-6000, using CuK radiation (λ = 0.15406 nm), operated at 40 kV and 30 mA, scanning from 20° to 60°, with a speed of 2°/min at 0.02° intervals and a time of 0.6 s.

The X'pert Panalytical High Score Plus software and the JCPDS (Joint Committee on Powder Diffraction and Standards) database were used to identify and quantify the phases. Crystallinity was determined from the ratio between the integrated area of the peak referring to the crystalline phase and the area referring to the amorphous fraction, using the Shimadzu Crystallinity software. Finally, the average size of the crystallites of the CaP nanoparticles was obtained using the width at half height of the diffractogram peaks, using the Scherrer equation [14]:

$$D = \frac{K \cdot \lambda}{\beta \cdot cos\theta} \quad (1)$$

In the formulation, D corresponds to the average size of the crystallite. K is a constant that depends on the experimental setup used and the geometry of the sample, which in this case corresponds to 0.90. λ is the wavelength of the incident radiation, which in this case is 0.15, referring to the wavelength of the copper anode. β is the width at half height of the diffraction peaks (FWHM—Full Width at Half Maximum), and θ is the diffraction angle of the crystalline plane or Bragg angle. Fourier transform infrared spectroscopy (FTIR) was performed to identify the functional groups in a BunKer model TENSOR 27 spectrometer with a range of 4000 to 400 cm^{-1}. The analysis was performed using pellets

containing the sample powder and spectroscopic grade KBr in the proportion of 0.3 mg of powder to 300 mg of KBr (1%), with 64 accumulations. The pyrolyzed precursor samples at 400 ± 10 °C/1 h were also characterized by thermogravimetric analysis (TG/DTG) to evaluate the mass losses that occurred during heating. The analysis was performed in a thermal analyzer, model TA-60, from Shimadzu, with a heating rate of 10 °C/min, in a nitrogen atmosphere, using an alumina crucible and ambient temperature range (25 °C) up to a maximum temperature of 1000 °C. Scanning electron microscopy (SEM) was performed to analyze morphological aspects in a microscope of the brand FEI COMPANY, model Quanta FEG 250, with accelerating voltage from 1 to 30 kV.

2.4. Biological Tests

Staphylococcus aureus (ATCC 25923) and *Escherichia coli* (ATCC 25922) bacterial strains of Gram-positive and Gram-negative species were used, respectively.

Cultures were obtained by transferring a bacterial growth colony from nutrient agar to a sterile falcon tube containing 3.0 mL of Brain Heart Infusion (BHI) broth, followed by incubation at 37 °C for 24 h. The bacterial inoculum used in the bioassays was prepared in a suspension, transferring 1.0 mL of the culture to a falcon tube containing 9.0 mL of the BHI medium.

BCP-40, BCP-50, and BCP60 were tested separately against *S. aureus* and *E. coli* in triplicates. The direct contact test in a solid medium was performed according to Zheng and Zhu [15]. AN amount of 100 µg of BCP was mixed with 100 µL of bacterial suspension (inoculum), standardized by the McFarland scale at 1.5×10^8 colony-forming units per mL (CFU/mL). After, they were transferred to Petri dishes containing the agar medium Mueller Hinton and seeded with the aid of a Drigalski loop, followed by incubation at 37 °C for 24 h. Only the bacterial inoculum was seeded on the plates as a positive control.

The inhibitory effect produced by each test solution was calculated according to Equation (2):

$$\eta = \frac{N1 - N2}{N1} * 100\ \% \quad (2)$$

where η is defined as the inhibitory effect, $N1$ is the arithmetic mean of the colony-forming units of the control plates, and $N2$ is the arithmetic mean of the colony-forming units of each of the samples tested.

3. Results

Figure 2 shows the formation of a biphasic calcium phosphate ceramic, in all synthesized samples, with characteristic peaks of the HAp phase (standard card JCPDS 009-0432) and the β-tricalcium phosphate phase (standard card JCPDS 009-0169). It is observed, for all samples, that the increase in the AC/EG ratio caused the reduction of the β-TCP peaks, for example, in the peaks 27.80° (2 1 4), 31.07° (2 1 0), and 32.42° (1 2 8), 34.23° (2 2 0), favoring the increase of the HAp phase formed.

Table 1 shows the results of the samples' quantification of phases, crystallite size, and crystallinity.

Table 1. Quantification of phases, crystallite size, and degree of crystallinity of the samples.

Quantification of the Phases (%)			HAp Crystallite Size (nm)	Degree of Crystallinity (%)
Sample	**HAp**	**β-TCP**		
BCP-60	98	02	63.1	94.8
BCP-50	45	55	61.1	88.1
BCP-40	39	61	60.6	82.3

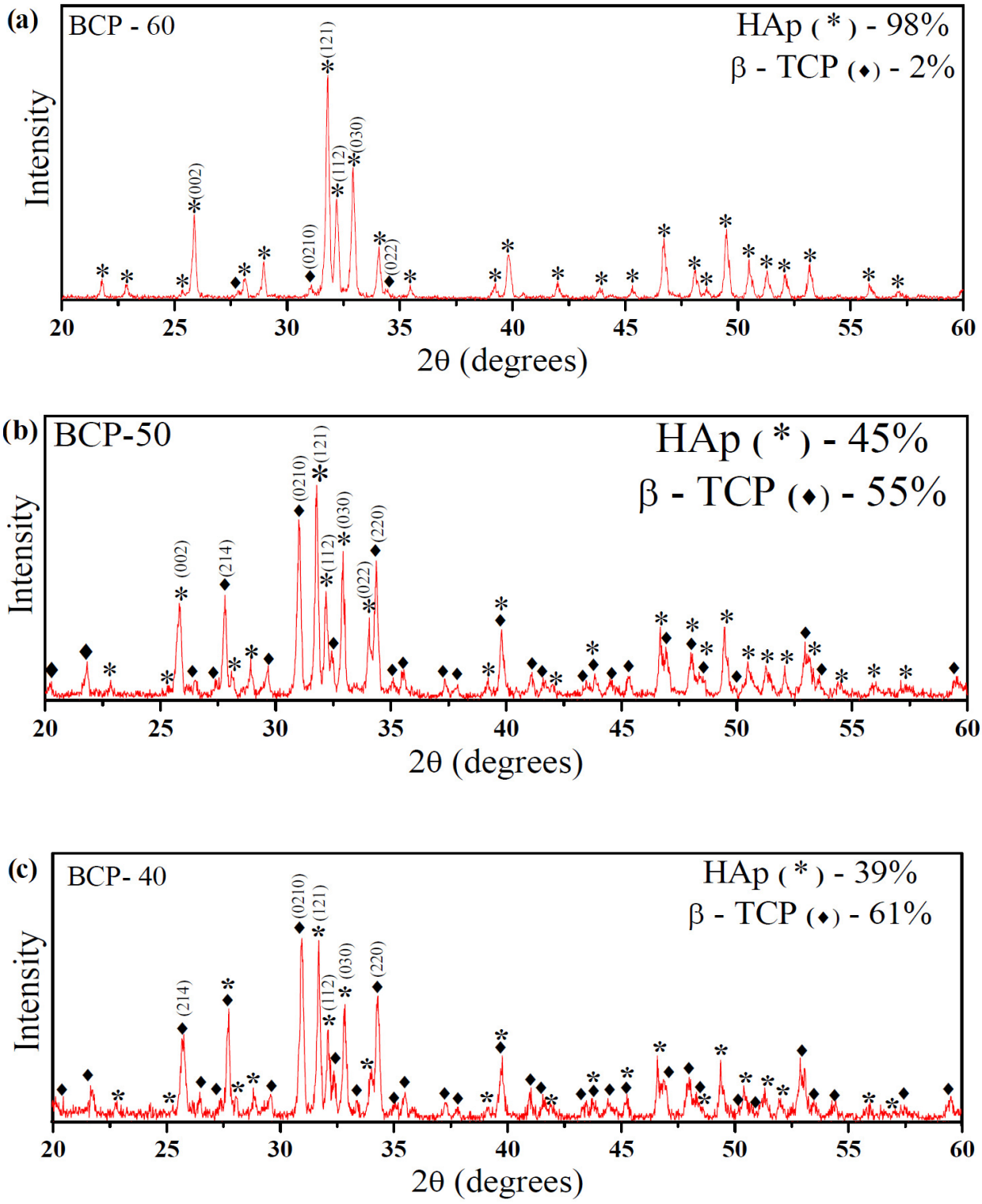

Figure 2. X-ray diffractograms of the synthesized samples BCP-60 (**a**), BCP-50 (**b**), and BCP-40 (**c**), varying the AC/EG ratio in the proportions of 60/40, 50/50, and 40/60, respectively.

The average crystallite sizes ranged from 60.6 to 63.1 nm, evidencing the nanometric character of the particles, in agreement with the literature [16–19]. In addition, all samples showed high crystallinity values, ranging from 82.3 to 94.8%, where these increased as the proportion of citric acid in ethylene glycol increased.

Figure 3 shows the infrared spectra of samples BCP-60 (a), BCP-50 (b), and BCP-40 (c). From the FTIR analysis, there are four main functional groups in the samples: OH^- PO_4^{3-}, CO_3^{2-}, and HPO_3^{4-}.

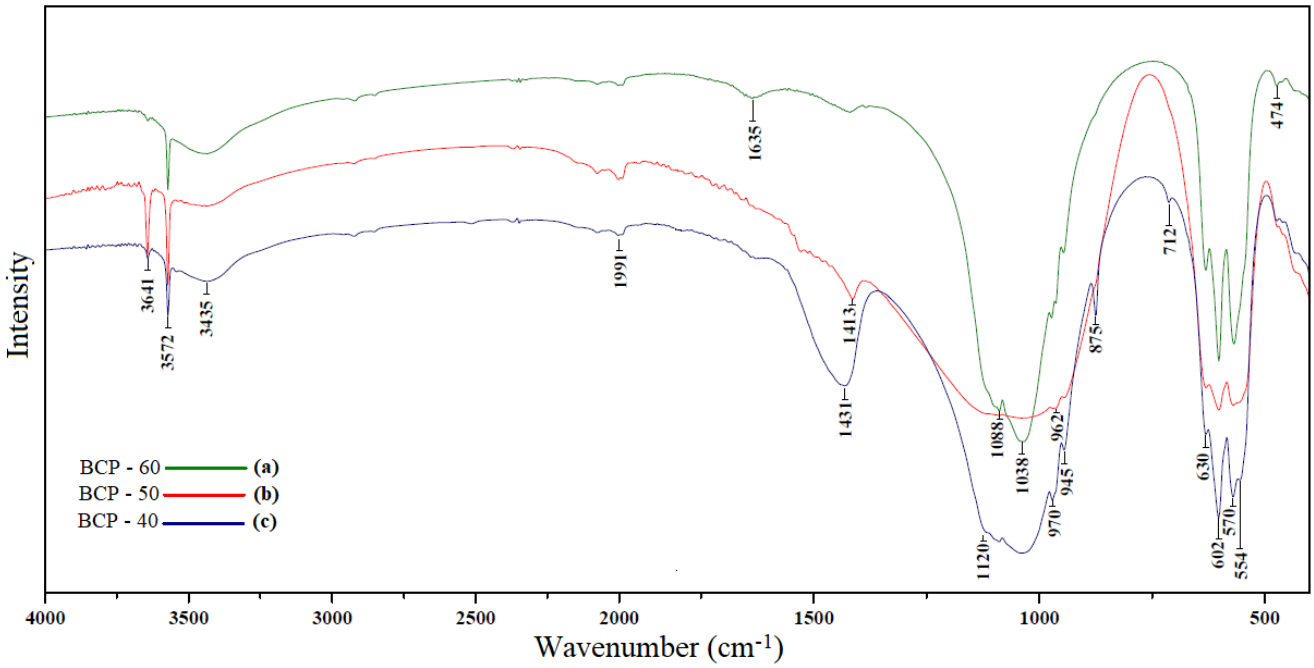

Figure 3. Infrared spectra of BCP-60 (**a**), BCP-50 (**b**), and BCP-40 (**c**).

The prominent bands that prove the presence of HAp and do not appear in the β-TCP phase are 3572 and 630 cm^{-1}. They are referenced to the stretching and vibration modes of the structural groups (OH) on the lattice of the HAp crystallite, respectively. In addition, the band at 3641 cm^{-1} probably belongs to calcium hydroxide, $Ca(OH)_2$. The bands 3435 and 1635 cm^{-1} confirm the presence of water molecules adsorbed in the samples [20,21].

The bands of PO_4^{3-}, a group of the HAp phase, occur at 1088, 1038, 962, 602, 554, 570, and 474 cm^{-1}. The bands 1088 and 1038 cm^{-1} correspond to the vibration mode ν3. (P-O), 602 and 570 cm^{-1} symmetrical and asymmetrical deformation in the plane (ν4 O-P-O). The bands 554 and 474 cm^{-1} are flexural O-P variations of the mode (ν2) of the PO_4 group (ν2 -O) [6,22,23]. On the other hand, the band at 875 cm^{-1} belongs to a carbonate group.

As the amount of the HAp phase increases (from the BCP-40 to the BCP-60), there was a reduction in bands 1120, 970, and 945 cm^{-1}, which corresponds to the BCP.

Figure 4 presents two mass loss events for the three analyzed samples. The events occurred in similar temperature ranges for all samples, referring to the same mass losses. The first event occurred at a temperature of 422 °C for the BCP-60, 376 °C for the BCP-50, and 381 °C for the BCP-40, corresponding to the combustion of the organic matter present in the material, resulting from citric acid and ethylene glycol. An initial process of dehydroxylation may occur with the exit of water. In this first event, the mass losses were approximately 1% for all samples.

The second event occurred with maximum decomposition temperatures of 618, 548, and 616 °C for BCP-60, BCP-50, and BCP-40, respectively, and is related to the formation of BCP. The mass losses for the second event were approximately 6.5% for the BCP-60, 5.8% for the BCP-50, and 4.3% for the BCP-40.

Figure 5 presents the electronic microscopy of the samples, showing the particular morphology of each synthesized sample.

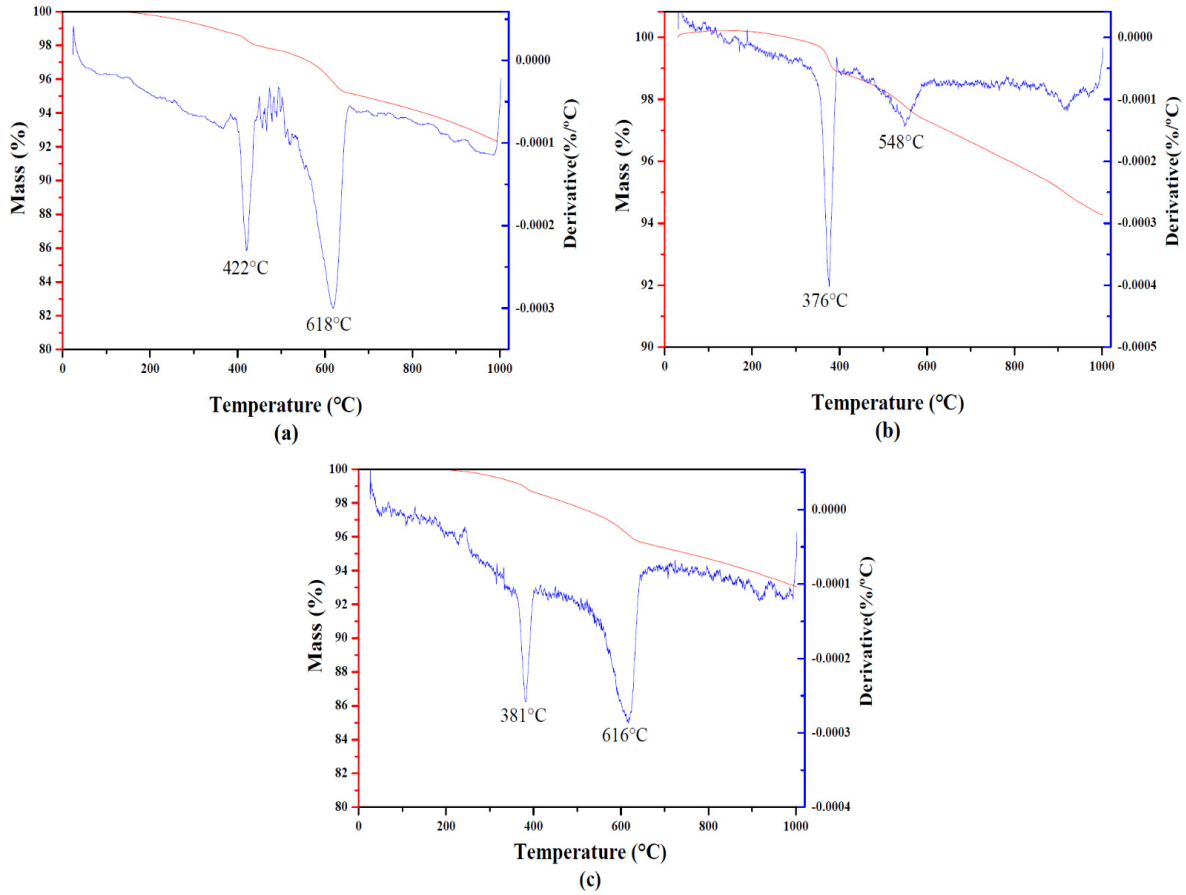

Figure 4. Thermogravimetric curves (TG/DTG) of BCP-60 (**a**), BCP-50 (**b**), and BCP-40 (**c**).

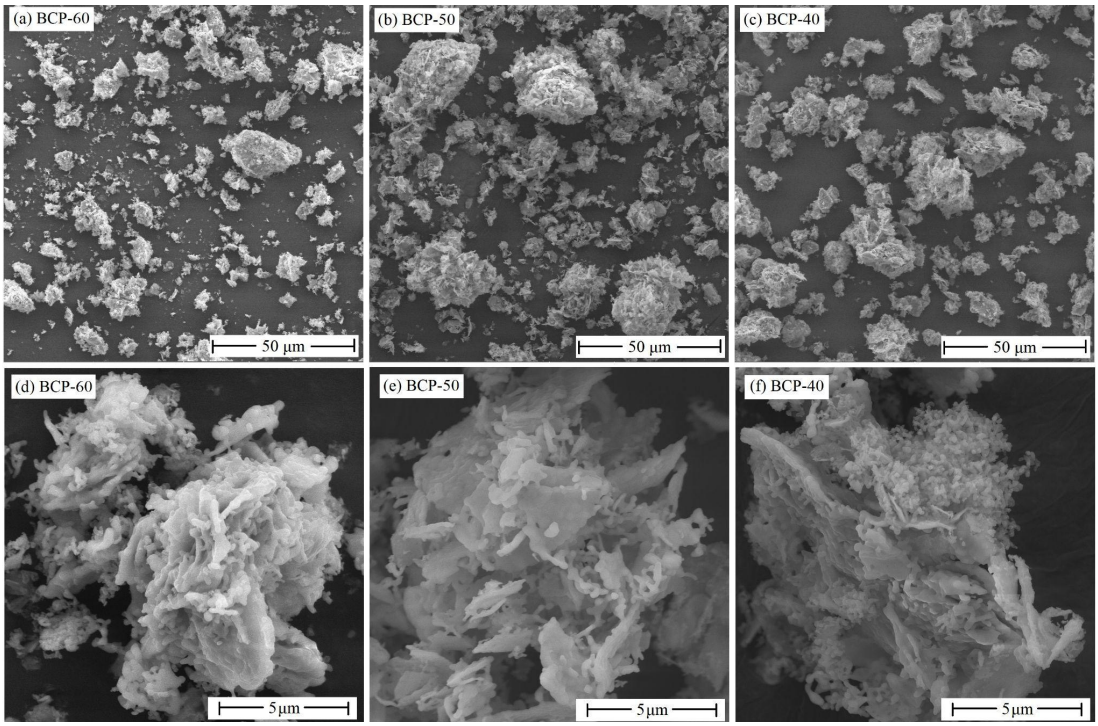

Figure 5. SEM of BCP-60, BCP-50, and BCP-40.

The micrographs show the particles are grouped, forming agglomerates with irregular shapes, showing heterogeneity of the two phases, HAp and β-TCP. The powders essentially show a mixture of particles of different sizes. However, it is possible to observe the presence of two different shapes of particles: larger plates (possibly referring to the β-TCP phase) and rods (very characteristic of the HAp phase) [24,25].

Samples BCP-60, BCP-50, and BCP-40 had their antimicrobial activity tested against Gram-positive (*Staphylococcus Aureus*) and Gram-negative (*Escherichia coli*) microorganisms.

Figure 6 shows the result of the microbiological tests for the two bacteria used in different proportions.

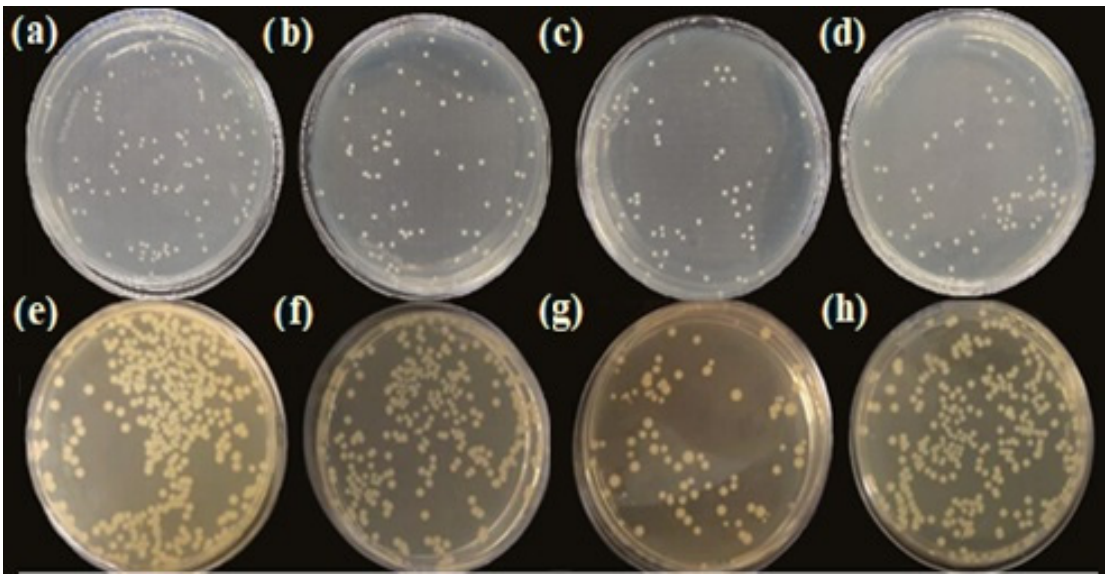

Figure 6. Images of microbiological tests: (**a**) *Staphylococcus aureus* (SA) control, (**b**) inhibitory effect of BCP-60 against SA, (**c**) inhibitory effect of BCP-50 against SA, (**d**) BCP-40 inhibitory effect against SA, (**e**) *Escherichia coli* (EC) control, (**f**) BCP-60 inhibitory effect against EC, (**g**) BCP-50 inhibitory effect against EC, (**h**) BCP-40 inhibitory effect against EC.

It is possible to verify that the bacterial growth was different in the tests against *S. aureus* and *E. coli* within the samples of BCP. In assays using *S. aureus*, bacterial growth was 43.10% lower when using BCP-50. In tests against *E. coli*, growth inhibition was 73.39% when using BCP-50 concentration. Comparing the three samples, the BCP-50 was better in the tests with the two bacterial strains.

The percentages of reduction in bacterial colony growth are listed in Table 2.

Table 2. Percentage of inhibition of bacterial growth.

Sample	*Staphylococcus aureus* (% of Inhibition)	*Escherichia coli* (% of Inhibition)
BCP-60	35.34	38.06
BCP-50	43.10	73.39
BCP-40	30.17	25.07

4. Discussion

The increase in the quantification of the HAp phase in the samples is probably due to the increase in the citric acid content in the solution because it has three carboxylic groups (-COOH) in its composition, which in solution become citrate ions due to the loss of a proton and a hydroxyl (OH-). Such groups act as a chelating agent, sequestering a greater amount of metal ions in the solution and forming a complex, thus preventing the segregation of

PO_4^{-3} ions, favoring the formation of stoichiometric HAp, with a Ca/P = 1.67 ratio [26–29]. On the other hand, with the decrease in the AC/EG ratio, the amount of citric acid decreased, which generated an insufficient homogeneity in the distribution of ions and a decrease in the Ca/P ratio of the samples, resulting in the formation of more β-TCP. The results suggest that the citric acid content significantly influences the formation of phases [29]. Moreover, it corroborates the studies by Omori et al. [6], who reported the influence of AC-EG resin on the Ca/P ratio of Hap samples. Roopalakshmi et al. [16] also stated that the β-TCP phase might occur due to the poor complexity of the PO_4^{3-} group, caused by the inefficient homogeneity of the solution or the short reaction time of the precursors with citric acid.

The characteristic bands for the phosphate group (PO_4^{-3}) of the β-TCP phase appeared at 1120, 970, and 945 cm^{-1}, with 1120 asymmetric elongation (ν3 P-O), 970 and 945 cm^{-1} symmetric elongations (ν1 P-O) [8,30]. In addition, the bands 1991, 1431, and 1413 cm^{-1} confirm the presence of carbonate groups (CO_3^{2-}) in the samples. Furthermore, the band at 1413 cm^{-1} is related to the symmetric stretching of the C-O group (ν3) cm^{-1}.

The reduction of bands from the BCP-40 sample to BCP-60 confirms the decrease in the β-TCP phase and increase in crystallinity and crystallites. The FTIR analysis confirms that the samples synthesized showed the functional groups of the HAp and β-TCP phases, corroborating the results of the XRD patterns.

The thermal behavior of all samples was similar, where all showed good thermal stability, with low mass losses, which were 7.73, 6.97, and 5.74% for samples BCP-60, BCP-50, and BCP-40, respectively. Furthermore, the low percentage of total mass loss of the samples is significant because thermal stability is crucial in controlling sintering or thermal processing conditions for the design and preparation of ceramics [31].

The antimicrobial activity of the samples was tested against two strains of bacteria, one Gram-positive and the other Gram-negative, obtaining a degree of inhibition of both bacteria. This test was essential to evaluate the interaction of samples with microorganisms that commonly cause community and hospital infections, the latter being closely related to surgical procedures [32].

It is known that ceramic materials such as CaP have physicochemical properties and are very similar to the natural composition of dental tissue and other bones in the human body. Therefore, using these materials in surgical procedures can be a gain for medicine, as the organism accepts it well, does not present toxicity, and does not favor bacterial growth [33,34].

When samples BCP-60, BCP-50, and BCP-40 were used, a linear trend of growth inhibition was not seen, with BCP-50 being better than the other samples. This behavior can be explained by a possible plateau of electrostatic forces interacting with microorganisms. Even so, the interaction and inhibition are better in the *E. coli* strain [35,36].

The mechanism generally explains the antibacterial properties of solid-state materials based on the electrostatic interaction between the bacterial cell wall and the metal ions in the HAp/β-TCP molecules [35]. In this way, bacteria move towards surfaces coated with HAp/β-TCP particles. In addition, metal ions interact with the microbial membrane and induce structural and permeability changes [37–40]. Thus, metal ions can interact with microbial nucleic acids, preventing microbial replication, possibly occurring more satisfactorily in the BCP-50 sample with 73.39% inhibition for the growth of *E. coli* bacteria and 43.10% for *S. aureus*. The results of this test were satisfactory. BCP can be used as a promising material for biotechnological use in surgeries.

5. Conclusions

This study aimed to produce calcium phosphates via the Pechini method, where the method was efficient in obtaining the biphasic ceramic formed by hydroxyapatite and beta-tricalcium phosphate, producing samples with different concentrations of the two phases depending on the AC/EG variations used in the synthesis. As a result, the two-phase ceramic obtained characteristics of nanometric powders, with a high degree

of crystallinity, total mass losses of approximately 7%, and agglomerated particles of irregular shape. Furthermore, regardless of the HAp/β-TCP concentration, the samples demonstrated inhibitory effects on the growth of the bacteria tested, with the BCP-50 sample being more effective against *E. coli.* The study indicates that BCP can be explored in several biotechnological fields that use ceramic materials in surgical procedures. Due to its physicochemical properties, living organisms are very accepted and do not favor the proliferation of microorganisms, mainly Gram-negative ones, which prevents post-surgical infections.

Author Contributions: Conceptualization, G.K.C. and I.S.L.; methodology, G.K.C., J.R.S.F., I.S.L., G.A.N. and R.M.; software, G.A.N. and R.M.; validation, G.A.N. and R.M.; investigation, G.K.C.; resources, E.C.S.-F.; writing—original draft preparation, G.K.C.; writing—review and editing, A.M.N. and J.A.O.; visualization, A.M.N., J.A.O. and A.B.; supervision, J.A.O., A.B. and E.C.S.-F.; project administration, J.A.O., A.B. and E.C.S.-F.; funding acquisition, E.C.S.-F. All authors have read and agreed to the published version of the manuscript.

Funding: This research received no external funding.

Data Availability Statement: Not applicable.

Acknowledgments: The authors thank CAPES, CNPq, and UFPI.

Conflicts of Interest: The authors declare no conflict of interest.

References

1. Munerato, M.S.; Biguetti, C.C.; Silva, R.B.P.; Silva, A.C.R.; Bacelar, A.C.Z.; Couto, M.C.R.; Duarte, M.A.H.; Santiago-Junior, J.F.; Bossini, P.S.; Matsumoto, M.A. Using different physicochemical biomaterials for oral and maxillofacial reconstruction, and inflammatory response and macrophage polarization. *Mater. Sci. Eng. C* **2020**, *107*, 110229. [CrossRef] [PubMed]
2. Nihouannen, D.L.; Daculsi, G.; Saffarzadeh, A.; Gauthier, O.; Delplace, S.; Pilet, P.; Layrolle, P.; Araújo, D.S.; Diniz, V.C.S.; Dantas, J.; et al. Avaliação da fotoluminescência do TiO_2 sintetizado pelo método Pechini. *Cerâmica* **2017**, *63*, 367.
3. Kolk, A.; Handschel, J.; Drescher, W.; Rothamel, D.; Kloss, F.; Blessmann, M.; Heiland, M.; Wolff, K.-D.; Smeets, R. Current trends and future perspectives of bone substitute materials–From space holders to innovative biomaterials. *J. Cranio-Maxillofac. Surg.* **2012**, *40*, 706–718. [CrossRef] [PubMed]
4. Zhu, Q.; Ablikim, Z.; Chen, T.; Cai, Q.; Xia, J.; Jiang, D.; Wang, S. The preparation and characterization of HA/β-TCP biphasic ceramics from fish bones. *Ceram. Int.* **2017**, *43*, 12213–12220. [CrossRef]
5. Nawang, R.; Hussein, M.Z.; Matori, K.A.; Abdullah, C.A.C.; Hashim, M. Physicochemical properties of hydroxyapatite/montmorillonite nanocomposite prepared by powder sintering. *Results Phys.* **2019**, *15*, 102540. [CrossRef]
6. Omori, Y.; Okada, M.; Takeda, S.; Matsumoto, N. Fabrication of dispersible calcium phosphate nanocrystals via a modified Pechini method under non-stoichiometric conditions. *Mater. Sci. Eng. C* **2014**, *42*, 562–568. [CrossRef]
7. Jiang, T.; Li, Z.; Xiao, P.; Cheng, Y.; Liu, Z.; Yu, S. Synthesis and growth mechanism of calcium phosphate layer on SiC-coated carbon/carbon composites with surface pre-oxidation. *Appl. Surf. Sci.* **2019**, *495*, 143427. [CrossRef]
8. Ebrahimi, M.; Botelho, M.G.; Dorozhkin, S.V. Biphasic calcium phosphates bioceramics (HA/TCP): Concept, physicochemical properties and the impact of standardization of study protocols in biomaterials research. *Mater. Sci. Eng. C* **2017**, *71*, 1293–1312. [CrossRef]
9. Aghayan, M.A.; Rodríguez, M.A. Influence of fuels and combustion aids on solution combustion synthesis of bi-phasic calcium phosphates (BCP). *Mater. Sci. Eng. C* **2012**, *32*, 2464–2468. [CrossRef]
10. Ruiz-Aguilar, C.; Olivares-Pinto, U.; Aguilar-Reyes, E.A.; López-Juárez, R.; Alfonso, I. Characterization of -tricalcium phosphate powders synthesized by sol–gel and mechanosynthesis. *Boletín De La Soc. Española De Cerámica Y Vidr.* **2018**, *57*, 213–220. [CrossRef]
11. Rodella, C.B.; Nunes, L.A.O.; Saeki, M.J.; Padilha, P.M.; Florentino, A.O. Caracterização textural e estrutural de V2O5/TiO2 obtidos via sol-gel: Comparação entre secagem convencional e supercrítica. *Química Nova* **2002**, *25*, 209–213. [CrossRef]
12. Agrawal, K.; Singh, G.; Puri, D.; Prakash, S. Synthesis and Characterization of Hydroxyapatite Powder by Sol-Gel Method for Biomedical Application. *J. Miner. Mater. Charact. Eng.* **2011**, *10*, 727–734. [CrossRef]
13. Arokiasamy, P.; Abdullah, M.M.A.B.; Rahim, S.Z.A.; Luhar, S.; Sandu, A.V.; Jamil, N.H.; Nabiałek, M. Synthesis methods of hydroxyapatite from natural sources: A review. *Ceram. Int.* **2022**, *48*, 14959–14979. [CrossRef]
14. Galea, L.; Bohner, M.; Thuering, J.; Doebelin, N.; Ring, T.A.; Aneziris, C.G.; Graule, T. Growth kinetics of hexagonal submicrometric β-tricalcium phosphate particles in ethylene glycol. *Acta Biomater.* **2014**, *10*, 3922–3930. [CrossRef] [PubMed]
15. Owens, G.J.; Singh, R.K.; Foroutan, F.; Alqaysi, M.; Han, C.M.; Mahapatra, C.; Kim, H.W.; Knowles, J.C. Sol–gel based materials for biomedical applications. *Prog. Mater. Sci.* **2016**, *77*, 1–79. [CrossRef]

16. Panda, S.; Biswas, C.K.; Paul, S. A comprehensive review on the preparation and application of calcium hydroxyapatite: A special focus on atomic doping methods for bone tissue engineering. *Ceram. Int.* **2021**, *47*, 28122–28144. [CrossRef]
17. Peña, J.; Vallet-Regı, M. Hydroxyapatite, tricalcium phosphate and biphasic materials prepared by a liquid mix technique. *J. Eur. Ceram. Soc.* **2003**, *23*, 1687–1696. [CrossRef]
18. Scherrer, P. Nachrichten von der Gesellschaft der Wissenschaften zu Gottingen. *Math.-Phys. Kl.* **1918**, *2*, 98–100.
19. Zheng, L.Y.; Zhu, J.F. Study on Antimicrobial Activity of Chitosan with Different Molecular Weights. *Carbohydr. Polym.* **2003**, *54*, 527–530. [CrossRef]
20. Roopalakshmi, S.; Ravishankar, R.; Belaldavar, S.; Prasad, R.G.S.V.; Phani, A.R. Investigation of Structural and Morphological Characteristic of Hydroxyapatite Synthesized by Sol-Gel Process. *Mater. Today Proc.* **2017**, *4*, 12026–12031. [CrossRef]
21. Stötzel, C.; Müller, E.A.; Reinert, E.; Niederdraenk, E.; Barralet, J.E.; Gbureck, U. Ion adsorption behavior of hydroxyapatite with different crystallinities. *Colloids Surf. B Biointerfaces* **2009**, *74*, 91–95. [CrossRef] [PubMed]
22. Gao, S.; Sun, R.; Wei, Z.; Zhao, H.; Li, F., II. Size-dependent defluoridation properties of synthetic hydroxyapatite. *J. Fluor Chem.* **2009**, *130*, 550–556. [CrossRef]
23. Dorozhkin, S.V. Bioceramics of calcium orthophosphates. *Biomaterials* **2010**, *31*, 1465–1485. [CrossRef] [PubMed]
24. Patai, P.; Futalan, C.M.; Utara, S.; Khemthong, P.; Kamonwannasit, S. Structural characterization of cerium-doped hydroxyapatite nanoparticles synthesized by an ultrasonic-assisted sol-gel technique. *Results Phys.* **2018**, *10*, 956–963.
25. Cimdina, L.B.; Borodajenko, N. *Research of Calcium Phosphates Using FourierTransform Infrared Spectroscopy, Infrared Spectroscopy-Materials Science, Engineering and Technology*; Intech: Shanghai, China, 2012; ISBN 978-953-51-0537-4.
26. Rameshbabu, N.; Kumar, T.S.S.; Prabhakar, T.G.; Sastry, V.S.; Murty, K.V.G.K.; Rao, K.P. Antibacterial nanosized silver substituted hydroxyapatite: Synthesis and characterization. *J. Biomed. Mater. Res. Part A* **2007**, *3*, 80. [CrossRef] [PubMed]
27. Iqbal, N.; Kadir, M.R.A.; Malek, N.A.N.N.; Mahmood, N.H.; Murali, M.R.; Kamarul, T. Rapid microwave-assisted synthesis and characterization of nanosized silver-doped hydroxyapatite with antibacterial properties. *Mater. Lett.* **2012**, *89*, 118–122. [CrossRef]
28. Piccirillo, C.; Pullar, R.C.; Tobaldi, D.M.; Castro, P.M.L.; Pintado, M.M.E. Hydroxyapatite and chloroapatite derived from sardine by-products. *Ceram. Int.* **2014**, *40*, 13231–13240. [CrossRef]
29. MashreghI, A.; Davoudi, F. The effect of ethylene glycol/citric acid molar ratio in the initial precursor of TiO2 nanoparticle paste synthesized by a polymerizable complex method on the photovoltaic properties of dye-sensitized solar cells. *Mater. Sci. Semicond. Processing* **2015**, *30*, 618–624. [CrossRef]
30. Guo, R.; Huang, J.; Chen, X.; Luo, Q.; Luo, L.; Xiong, Y.; Zhang, S. Pechini sol-gel synthesis of $La_2CaB_8O_{16}$:Eu^{3+} red phosphor and its photoluminescence spectral properties. *J. Lumin.* **2019**, *206*, 15–20. [CrossRef]
31. Bakar, S.N.A.; Talib, I.A.; Osman, N. The effect of different molar ratio citric acid and ethylene glycol to metal cation on the ceramics powder of Y^{3+} doped $BaZrO_3$. *Solid State Sci. Technol.* **2010**, *18*, 6936–6944.
32. Jouannaux, J.; Haeussler, A.; Drobek, M.; Ayral, A.; Abanades, S.; Julbe, A. Lanthanum manganite perovskite ceramic powders for CO_2 splitting: Influence of Pechini synthesis parameters on sinterability and reactivity. *Ceram. Int.* **2019**, *45*, 15636–15648. [CrossRef]
33. Karampas, I.A.; Kontoyannis, C.G. Characterization of calcium phosphates mixtures. *Vib. Spectrosc.* **2013**, *64*, 126–133. [CrossRef]
34. Tõnsuaadu, K.; Gross, K.A.; Pluduma, L.; Veiderma, M. A review on the thermal stability of calcium apatites. A review on the thermal stability of calcium apatites. *J. Therm. Anal. Calorim.* **2012**, *110*, 647–659.
35. Schnieders, J.; Gbureck, U.; Vorndran, E.; Schossig, M.; Kissel, T. The effect of porosity on drug release kinetics from vancomycin microsphere/calcium phosphate cement composites. *J. Biomed. Mater. Res.* **2011**, *99*, 391–398. [CrossRef] [PubMed]
36. Mukai, M.; Uchida, K.; Sugo, K.; Nakasu, M.; Nakajima, T.; Takata, K.; Takaso, M.; Urabe, K. Long-term antibacterial activity of vancomycin from calcium phosphate cement in vivo. *Bio-Med. Mater. Eng.* **2022**, *33*, 41–50. [CrossRef]
37. Varma, P.R.H.; Fernandez, F.B. Bioceramics in Tissue Engineering: Retrospect and Prospects. In *Biomaterials in Tissue Engineering and Regenerative Medicine*; Springer: Singapore, 2021; pp. 61–87.
38. Erdem, U.; Dogan, M.; Metin, A.U.; Baglar, S.; Turkoz, M.B.; Turk, M.; Nezir., S. Hydroxyapatite-based nanoparticles as a coating material for the dentine surface: An antibacterial and toxicological effect. *Ceram. Int.* **2020**, *46*, 270–280. [CrossRef]
39. Stanić, V.; Dimitrijević, S.; Antić-Stanković, J.; Mitrić, M.; Jokić, B.; Plećaš, I.B.; Raičević, S. Synthesis, characterization and antimicrobial activity of copper and zinc-doped hydroxyapatite nanopowders. *Appl. Surf. Sci.* **2010**, *256*, 6083–6089. [CrossRef]
40. Oliveira, C.; Oliveira, A.L.M.; Chantelle, L.; Cavalcanti, G.R.S.; Landers, R.; Medina-Carrasco, S.; Orta, M.D.M.; Filho, E.C.S.; Jaber, M.; Fonseca, M.G. Functionalization of the hydroxyapatite surface with ZnO for alizarin immobilization. *Appl. Surf. Sci.* **2022**, *593*, 153412. [CrossRef]